Scholars' Mine

Masters Theses

Student Theses and Dissertations

Fall 2018

Coaxial cable ring resonator based on pair sided coaxial cable Bragg grating coupler for sensing appllication

Xiaotong Tang

Recommended Citation

COAXIAL CABLE RING RESONATOR BASED ON PAIR SIDED COAXIAL

CABLE BRAGG GRATING COUPLER FOR SENSING APPLICATION

by

XIAOTONG TANG

A THESIS

Presented to the Faculty of the Graduate School of the

MISSOURI UNIVERSITY OF SCIENCE AND TECHNOLOGY

In Partial Fulfillment of the Requirements for the Degree

MASTER OF SCIENCE IN ELECTRICAL ENGINEERING

2018

Approved by

Jie Huang, Advisor

Amardeep Kaur

Hongyan Ma

PUBLICATION THESIS OPTION

This thesis consists of the following article:

Paper I: Pages 7-29 are intended for submission to IEEE Sensors Journal

ABSTRACT

Coaxial cable based devices, such as coaxial cable Bragg grating (CCBG), coiled coaxial cable resonator have been demonstrated for sensing applications to address the challenges faced by fiber optic sensors (e.g., large strain survivability, installation). Inspired by the fiber ring resonator (FRR), coaxial cable based ring resonator (CCRR) is reported in this thesis. The device mainly formed by a homemade coaxial cable Bragg grating (CCBG) pair based side coupler. Comparing to the commercial coupler, CCBG-SC improves the flexibility of the device for sensing applications. The coupling frequency of the CCBG-based coupler can be modified by changing the grating length and period of the CCBG, providing a more convenient method to realize critical coupling in the CCRR. Resonances were observed at discrete frequencies in transmission spectrum. A high Q-factor could be achieved by varying the length of the loop. The basic principles were investigated to understand the device physics. The S-parameter of CCBG was calculated using finite element method. Full wave electromagnetic software was employed to simulate and demonstrate the concept. S-parameters of CCRR is calculated by an estimated algorithm. The device was tested for its potentially large strain application. The temperature responses were also investigated to study the influence of their crosstalk. CCRR sensing system offers improvements of performance and largely reduces costs by minimizing the requirements for insulation.

ACKNOWLEDGMENTS

I am appreciative of those people who helped me with the completion of my research for these two years.

First, I am grateful to my advisor, Dr. Jie Huang, without whom this research could be considered incomplete. I thank him for giving me a chance to work with the group, and also for his patience. He gave me lots of valuable suggestions so that I could improve my research.

I am grateful to Dr. Amardeep Kaur, Department of Electrical and Computer Engineering, and Dr. Hongyan Ma, Department of f Civil, Architectural and Environmental Engineering, for being my committee members.

I would like to thank all the group members including Chen Zhu, Yiyang Zhuang, Bohong Zhang, Muhammed Roman, who helped me solve problems all the time.

Finally, I would also like to thank my parents and friends for they support me always.

TABLE OF CONTENTS

LIST OF ILLUSTRATIONS

LIST OF ABBREVIATIONS

Abbreviation	Full name
SHM	Structural health monitoring
FOS	Fiber optic sensors
MEMS	Microelectromechanical systems
FBG	Fiber Bragg grating
OFDR	Optical frequency domain reflectometry
SNR	Signal-to-noise ratio
FRR	Fiber ring resonator
EM	Electromagnetic
RF	Radio frequency
CCFPI	Coaxial cable Fabry-Perot interferometer
CCBG	Coaxial cable Bragg grating
TDR	Time-domain reflectometry
CCRR	Coaxial cable ring resonator
POF	Plastic optical fiber
CCBG-SC	Pair-based side coupler
SRR	Split ring resonators
T-matrix	Transfer matrix
CNC	Computer numerical controlled
VNA	Vector network analyzer

1. INTRODUCTION

1.1. REVIEW OF SENSORS FOR SHM

The procedures and activities that researchers imply kinds of methods to detect damage of civil, aerospace and mechanical engineering infrastructure is called Structural Health Monitoring (SHM) [1]. Generally, the aim of SHM is to give a comprehensive diagnosis of different parts of the structure, structure assembly and the state of the constituting material [2]. With SHM, researchers can get the whole history of the structure and even get a prognosis (evolution of damage, residual life, etc.) [3]. These sensing systems include fiber optic sensors (FOS) such as fiber Bragg gratings (FBG), Fabry- Perot interferometer (FPI), Sagnac Interferometer and Mach-Zehnder Interferometer [4], Microelectromechanical system (MEMS) sensors (e.g. [5]), and wireless data acquisitions systems (e.g. [6]). For example, FBG, which is first proposed in 1978, has been widely applied in many structures with high sensitivity [7]. Another well-developed sensor, optical frequency domain reflectometry (OFDR), is also wildly explored and applied due to a higher signal-to-noise ratio (SNR) and spatial resolution [8]-[9]. This early monitoring of structure in a harsh environment can detect severe damage in concrete structures resulting from a loss of structural integrity and would allow appropriate action to be taken in advance to prevent major damage being caused and thus, saves lives and money [10].

      1.1.1. Fiber Optic Sensors. FOS has been wildly used in SHM for their advantages such as low loss, light weight, compactness, high resolution, high sensitivity, immunity to electromagnetic interference, and remote operation [11]. For example,

instead of mechanical spinning gyros, a closed-loop gyro was placed on the Delta Rocket in 1978 [12]. Since it has a great capability to a several of environment, the signal transmitting in fiber is smooth and reliable. There are mainly three types of FOS depending on the sensing range: local sensors, Quasi-distributed sensors, and distributed sensors. Depending on the objective of projects, researchers should choose different kinds of sensors. Take FBG as an example, FBG is one of the Quasi-distributed sensors. Comparing to other FOS, it is suitable to measure strain, displacement or pressure.

1.1.2.   Fiber Ring Resonator. Among these fiber optic sensors, fiber ring resonator (FRR) is one of the sensing structures that has been reported a lot due to its small size, low losses, and can be multiplied into optical networks [13]. Like other interferometric sensors (Sagnac forms, Mach-Zehnder, Michelson, Fabry-Perot or dual mode, polarimetric, grating and Etalon based interferometers.), optical ring resonator works on the modulation in the phase of light emerging from a single mode fiber. Back in 1982, L.F. Stokes and his group constructed the first all-fiber-ring resonator with a single-mode fiber and directional coupler [14]. Over the past thirty years, FRR has been demonstrated thoroughly and applied for its systematic manner. Due to constructive interference, the resonance will build up in multiple loop trip and then output to the output bus. FRR hold great promise for a variety of applications, including sensing, laser resonators, optical switching, photonic biosensors, optical time delay, add-drop filters, and frequency filtering [15].

However, FOS have limitations of fragile and small dynamic range. Fiber optic devices are easily broken when the strain is larger than 4000µm (0.4%), which makes it difficult to install and use these sensors for SHM. Moreover, fiber optic measurement

instrument is expensive. In this case, researchers studied several devices in order to find great solutions faced by FOS. Another sensing technique involves plastic optical fiber (POF) which can withstand higher strain up to 10% but have an extremely bad SNR, making it undesirable for large strain sensing [16].

1.2. REVIEW OF COAXIAL CABLE BASED SENSORS

To address the aforementioned limitations of fiber optic sensors, coaxial cable has been implied for sensing application in recent years. Being dominated by the same electromagnetics (EM) theory of fiber-optic, coaxial cables in radio frequency (RF) can also be implied in sensing field with the similar concept. Recently, a research group proposed a Coaxial cable Fabry-Perot interferometer (CCFPI) sensor with high spatial resolution and high finesse. It can be applied to temperature, strain and other types of applications [17]. Another example is a coaxial cable sensor based on time-domain reflectometry (TDR) for crack sensing in the concrete structure was proposed. By modifying the topology of cable, they could largely improve the sensitivity of cable sensor [18].

1.3. NOVEL CCRR DEVICE FOR SHM

Inspired by FRR, coaxial cable ring resonator (CCRR) based on a pair of CCBG has been proposed in this paper since they share several same physics principles. By controlling the length of the ring resonator, the parameters can be identified by how they vary between devices. CCRR offers superior advantages over FRR such as immunity to surroundings interference and large bandwidth. Furthermore, Coaxial cable ring resonator

can withstand large strains, offers better temperature stability and enables large distance deployment.

Comparing to the optical fiber, coaxial cable can be bent in any shape. It is easy to control or implement and it might also be low cost. Due to these superior structural benefits, CCRR has a great potential in SHM. In this way, CCRR can be used for large strain sensing which has a loop of several meters in length to be operated as an axial strain sensor due to their huge differences in source wavelength. The change in applied temperature or large strain to sensing part may lead to change of the material properties or the physical length of the conductor and insulator of the cable ring, leading to the change of the shift of spectra. Since an intact coaxial cable could be used in strain sensing without any hole-breaking, CCRR might be a good large strain sensor, which is well shaped by the structure of CCBG device. Some researchers have already studied the characteristics of CCRR. Pan et.al have already proposed the algorithm to calculate the S-parameter of CCRR. The system is composed of coaxial cables and a commercial directional coupler. The proposed algorithm agrees well with the measurement response [19]. However, due to the limitation of a directional coupler, the coupling coefficient can't be changed, leading to a low efficiency for sensing application. Coaxial cable Bragg Grating (CCBG) was first demonstrated in 2012 inspired by well-known fiber Bragg Grating (FBG) [20]. By setting two CCBG in parallel, electromagnetic field coupling can be observed through this CCBG pair-based side coupler (CCBG-SC) [21]. The coupling frequency and strength can be changed though grating period and length. Therefore, CCBG coupler has more flexibility than normal commercial directional coupler.

In this thesis, the CCRR device is presented through a CCBG-SC for strain and temperature sensing applications. Using the S-parameter estimated method, the theory of the system can be analyzed. A combination of simulations of CCBG-SC and CCRR using full wave electromagnetic software are also given. The results of experiment verify the concept of coaxial cable ring resonator. Using CCRR as a sensor testing large strain and temperature is also presented. The results show that the CCRR sensor is sensitive to strain and temperature with respect to frequency. Although in this thesis, the CCRR only used to measure temperature and large strain. The CCRR device has a great potential and can also be used to measure kinds of parameters in SHM such as pressure, liquid level, and displacement.

2. RESEARCH OBJECTIVE

From the discussion above, the main objective of this thesis is to setup CCRR system for measure parameters in SHM. To be detailed, the specific objectives are to:

1) Investigate the fundamental physics and theoretical model of the device.

2) Investigate the optimal techniques and processes to generate the periodic discontinuities of CCBG.

3) Investigate the optimal setup to make a high quality CCRR device.

4) Demonstrate the device for temperature and large strain measurement and investigate the relationship of temperature/strain and transmission spectrum of CCRR.

PAPER

I. COAXIAL CABLE RING RESONATOR BASED ON PAIR SIDED COAXIAL CABLE BRAGG GRATING COUPLER FOR SENSING APPLICATION

ABSTRACT

Coaxial cable based devices, such as coaxial cable Bragg grating (CCBG), coaxial cable Fabry-Perot interferometer/resonator (CCFPI/CCFPR), have been demonstrated for sensing applications in recent years. Inspired by the fiber ring resonator (FRR), coaxial cable ring resonator (CCRR) is proposed in this paper. A homemade coupler, i.e., a pair of coaxial cable Bragg grating (CCBG) aligned in parallel, is employed to construct the CCRR. The coupling frequency of the CCBG-based coupler can be modified by changing the grating length and period of the CCBG, providing a more convenient method to realize critical coupling in the CCRR. The basic principles were investigated to understand the device physics. Full wave electromagnetic software was employed to simulate and demonstrate the concept. Large strain and temperature responses of a prototype device were tested.

1. INTRODUCTION

In past two decades, fiber optic sensors have been widely used from laboratory experiments to real-world applications due to their unique advantages, such as lightweight, low loss, high resolution, electromagnetic interference, capabilities for distributed sensing and remote operation [1]. A lot of sensor structures based on different principles have been proposed and demonstrated for physical and chemical parameter sensing. Examples include fiber Bragg grating (FBG) [2], long-period grating [3], Fabry-Perot Interferometer Sensor [4], Sagnac Interferometer Sensor [5], and Mach-Zehnder Interferometer Sensors [6], all of which have been explored to realize highly-sensitive strain measurements. For example, thousands of FBGs have been cascaded in an optical fiber to measure the strain profile of the optical fiber for structural health monitoring (SHM)Another widely demonstrated sensing structure, ring resonator, has been studied for several decades no matter optical or microwave regions [7]-[9]. It consists of a waveguide in a closed loop coupled to one or more input/output waveguides. When electromagnetic (EM) wave of appropriate frequency is coupled to the loop by the input waveguide, it builds up in magnitude over multiple round-trips due to constructive interference. In optics, the length of the loop could be tens of or hundreds of micrometers due to the wavelength range of light source. Microsphere or micro ring resonators have been highly investigated for physical, chemical or biological sensing applications [10], [11]. For radio frequency (RF) region, split ring resonators (SRR) have been fully analyzed and experimentally demonstrated [12], which could be used to produce a negative magnetic permeability material. In recent years, SRRs have been used, which is

made by producing some splits in a pair of closed loops, for the fabrication of sensors especially in terahertz region [13].

Governed by the same EM theory, coaxial cables and optical fibers have been widely used in communication area for transmitting signals along a long distance. In the past two decades, due to the fact that the frequencies (or wavelengths) of the EM waves supported by them are quite different, a lot of unique devices of their own have been developed. Compared to an optical fiber, a coaxial cable is larger in diameter and is much more robust, which is highly desired in SHM. For example, for strain measurement, fiber optic devices are fragile and can easily break when they are subject to a strain larger than about 4000 mε (0.4%) making it difficult to install and operate the sensors for structural health SHM.

Recently, we have successfully implemented some of fiber optic sensing concepts onto the coaxial cable to address the issues faced by fiber optic sensors (e.g., fragility, large strain survivability). The successful examples could be found in our previous studies including coaxial cable Bragg grating (CCBG) [15], coaxial cable Fabry-Perot interferometer [16], hollow coaxial cable Fabry-Perot resonator [17] and coiled coaxial cable resonator (CCCR) [18]. For example, CCBG, which is mimicking the optical counterpart, i.e., FBG, was fabricated by drilling holes into a coaxial cable in periodic spacing to introduce period impedance discontinuities. These impedance discontinuities generate weak reflections to the EM wave transmitting along the cable, resulting peaks/dips in reflection/transmission spectra at discrete frequencies. The prototype CCBG devices have been proved to be successful in large strain and liquid level and leakage measurements with large dynamic range and good robustness [19]. However, the

aforementioned coaxial cable based sensor devices have a relatively low quality-factor (Q-factor), which may limit their measurement resolution for sensing applications. Very recently, Pan et.al proposed the concept of coaxial cable ring resonator (CCRR) by mimicking the concept of the optical ring resonator [20]. The CCRR was constructed by a common cable and a directional coupler. Unlike the fiber ring resonators, CCRR could have a loop of several meters in length to be operated as an axial strain sensor due to their huge differences in source wavelength. A higher Q factor also could be achieved as the length of the loop increased. If the CCRR could also be used for large strain measurements in which an intact coaxial cable is used rather than a coaxial cable with many hole-breakings, it might become a promising candidate for extreme large strain sensing.

In this work, we have proposed a CCRR through a CCBG pair based side coupler (CCBG-SC) for large strain and temperature measurements. A homemade coupler, CCBG-SC is used instead of the commercial directional coupler to improve the flexibility of the device for sensing applications. By playing with the number of holes along CCBG-SC, the critical coupling can be reached. The coupling frequency can also be controlled by varying grating length or period of the CCBG-SC. The device physics was discussed. Full-wave simulations and an estimated algorithm were combined and performed to further understand the proposed device. In the demonstration experiments, large strain and temperature responses of the sensor were tested. The results showed that the proposed CCRR can survive up to 21 mε without cable breakage.

2. SIMULATION AND ALGORITHM

2.1. MODELING SETUP

Figure 1 shows a schematic diagram of the proposed CCRR system, which consists of a CCBG-SC and a ring of an intact coaxial cable. By setting two CCBG in parallel, CCBG based coupler is achieved. Similar to fiber optic, coaxial cable includes inner conductor, outer conductor, shield and a robust jacket. The performance of CCBG-SC is related to the number of holes and period of Bragg grating. Port 3 and port 4 connect to an intact coaxial cable to make a ring loop. When the wave coming, there are some portion of wave will transmit to port 2, while there are some portion of wave will be coupled to the ring resonator.
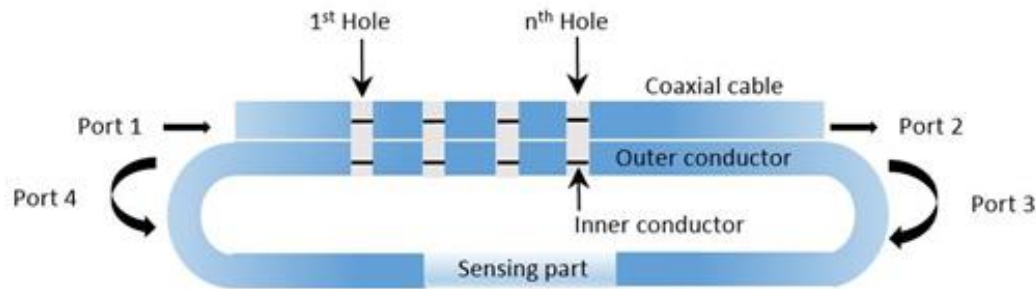
Figure 1. Schematic of CCRR based on CCBG-SC

2.2. PHYSICAL PRINCIPLE OF CCRR

The modeling method of the CCBG-SC can be found in our previous work [21], in which the CCBG-SC was modeled as series of discontinuities segments and transmission segments. We define the voltage input and output parameters of the discontinuity segment as a_1, a_2, a_3, a_4 and b_1, b_2, b_3, b_4 respectively, which is shown in Figure 2 (a). The four ports scattering parameter matrix of the discontinuity segment and transmission line segment are given as (1) and (2):

$$\begin{bmatrix} b_1 \\ b_2 \\ b_3 \\ b_4 \end{bmatrix} = S_{DS} \begin{bmatrix} a_1 \\ a_2 \\ a_3 \\ a_4 \end{bmatrix} = \begin{bmatrix} S_{11} & S_{12} & S_{13} & S_{14} \\ S_{21} & S_{22} & S_{23} & S_{24} \\ S_{31} & S_{32} & S_{33} & S_{34} \\ S_{41} & S_{42} & S_{43} & S_{44} \end{bmatrix} \begin{bmatrix} a_1 \\ a_2 \\ a_3 \\ a_4 \end{bmatrix} \tag{1}$$

$$\begin{bmatrix} b_5 \\ b_6 \\ b_7 \\ b_8 \end{bmatrix} = S_{TS} \begin{bmatrix} a_5 \\ a_6 \\ a_7 \\ a_8 \end{bmatrix} = \begin{bmatrix} 0 & e^{\Upsilon\Lambda} & 0 & 0 \\ e^{\Upsilon\Lambda} & 0 & 0 & 0 \\ 0 & 0 & 0 & e^{\Upsilon\Lambda} \\ 0 & 0 & e^{\Upsilon\Lambda} & 0 \end{bmatrix} \begin{bmatrix} a_5 \\ a_6 \\ a_7 \\ a_8 \end{bmatrix} \tag{2}$$

where S_{DS} is the S-matrix of the discontinuity segment, S_{TS} is the S-matrix of the transmission line segment, γ is the propagation constant and it is equal to $\alpha + i\beta$, where α is the attenuation constant of the cable and β is the phase constant, Λ is the distance between two holes, i e., the period of the CCBG.

To obtain the S-parameters of the segments, s4p matrices are calculated using a full-wave numerical solver (HFSS). Figure 2 (b) shows the simulation results of a discontinuity segment. As can be seen, the magnitude of the reflection/transmission coefficient increased/decreased as the interrogated frequency increased. Since

magnitudes of S31 and S41 of the discontinuity segment are same, the matrix of

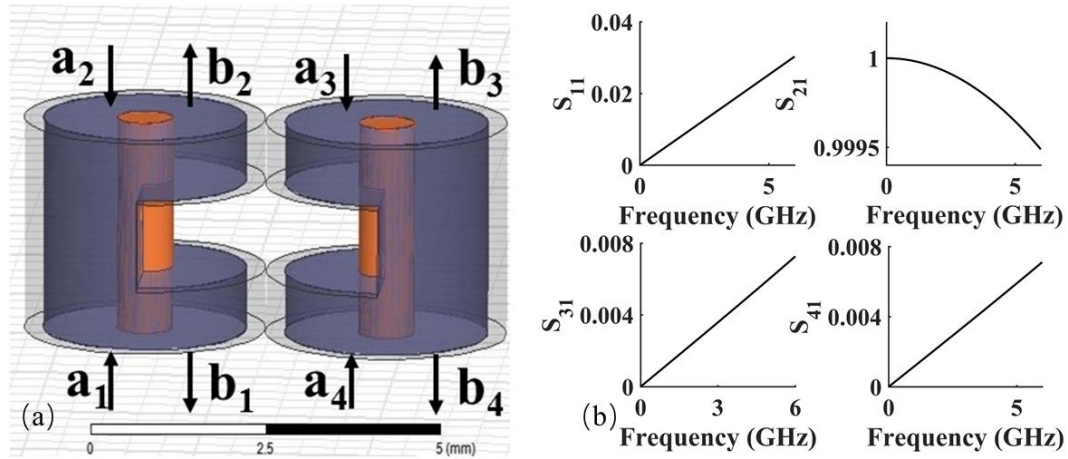discontinuity part is taken as symmetric which simplifies the calculation.

Figure 2. Simulation results of a hole in coaxial cable (a) Discontinuity section of the CCBG based coupler (b) Calculated S_{11}, S_{21}, S_{31}, and S_{41} of a discontinuity segment

Transfer matrix (T-matrix) is one solution that can express the cascading

relationship directly and it facilitates the mathematics of cascading multiple ports [22].

After wave propagates several discontinuity segments and transmission line segments,

the final equation about T-matrix is as following:

$$
\begin{bmatrix} b_1 \\ a_1 \\ b_4 \\ a_4 \end{bmatrix} = (T_{DS}T_{TS})^N \begin{bmatrix} a_{2N} \\ b_{2N} \\ a_{3N} \\ b_{3N} \end{bmatrix}
$$

(3)

where T_{DS} and T_{TS} are T-matrix of the discontinuity segment and transmission segment, respectively, N is the number of segments; a_{2N} b_{2N} are the Nth input and output voltages of CCBG. The next step is to convert T-matrix back to S-matrix to get the final relationship over four ports.

In the CCBG-SC calculation process, the dielectric of polyethylene, n, was set to be 2.25 and α was neglected. The calculation results of reflection, transmission and coupling coefficients of the CCBG-SC are shown in Figure 3 In the calculation, Λ is set to be 38mm and N is 133. Figure 3 (a) is the linear spectra of reflection coefficients (Γ) and transmission ratio (τ) and Figure 3 (b) is the linear spectra of coupling coefficients including forward coupling (κ_{fd}) from port 1 to port 3 and backward coupling (κ_{bd}) from port 1 to port 4. By understanding the theory in fiber Bragg gratings, it is easy to know that the forward propagating wave is coupled with the backward propagating wave. They have the same magnitude but opposite phases. The CCBG also satisfies the Bragg condition:

$$f_{res}^{m} = \frac{m}{2\Lambda\sqrt{LC}} \tag{4}$$

where f is the resonance frequency of the EM wave, m is an integer representing the order of grating. L and C are distributed inductance and capacitance of the cable. According to the datasheet of coaxial cable, C is 100 pF/m and L is 250 nH/m. As can be observed in Figure 3 (a). The two resonant frequencies are about 2.82 GHz and 5.64 GHz, which matches well with the Eq. (4). In Figure 3 (b), the coupling ratio (κ) reaches

a high coupling coefficient, which means that most of the energy can be transmitted to

the ring resonator at the discrete resonance frequencies. The forward coupling shows a

bad sideband suppression comparing to the backward coupling. The strength of resonant

peaks increases as the frequency increases. In theory, the coupling strength increases as

the number of grating points increases. The coupling bandwidth could also be changed by
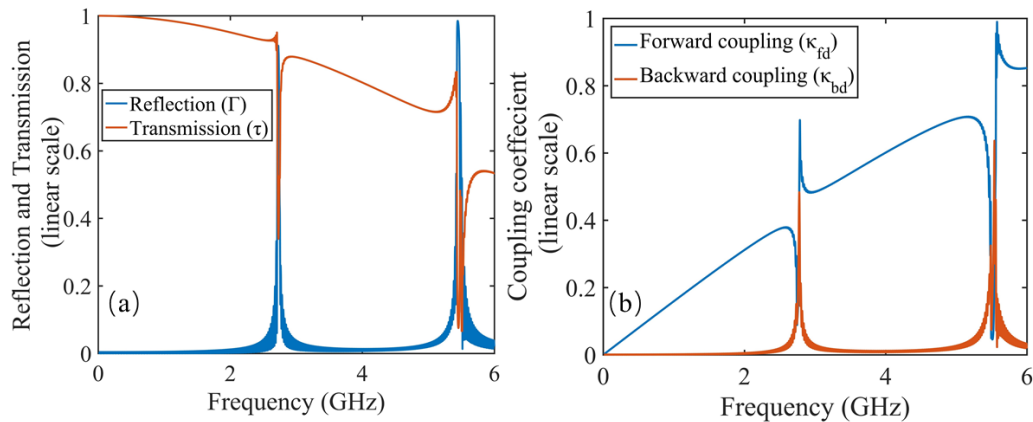
changing the shape structure of Bragg gratings [23].

Figure 3. Calculated spectra of CCBG (a) Spectra of reflection and transmission
coefficients of CCBG-SC (b) Calculated spectra of forward coupling and backward
coupling coefficients using T-matrix method

The coupler matrix can be expressed as a 4×4 matrix. The incident voltages and

reflection voltages are a_1, a_{2N}, a_3, a_{4N} and b_1, b_{2N}, b_3, b_{4N} respectively. The S-parameters

of the coupler can also be calculated using the same method. The relationship between

incident voltages and reflection voltages are:

$$\begin{bmatrix} b_1 \\ b_{2N} \\ b_{3N} \\ b_4 \end{bmatrix} = S_{coupler} \begin{bmatrix} a_1 \\ a_{2N} \\ a_{3N} \\ a_4 \end{bmatrix} = \begin{bmatrix} \Gamma & \tau & \kappa_{fd} & \kappa_{bd} \\ \tau & \Gamma & \kappa_{bd} & \kappa_{fd} \\ \kappa_{fd} & \kappa_{bd} & \Gamma & \tau \\ \kappa_{bd} & \kappa_{fd} & \tau & \Gamma \end{bmatrix} \begin{bmatrix} a_1 \\ a_{2N} \\ a_{3N} \\ a_4 \end{bmatrix} \tag{5}$$

To combine the matrix of a cable which is a 2×2 matrix, we define M, N, P, and Q to represent the four sub-matrices in the coupler and they can be expressed as (6) - (9):

$$M = \begin{bmatrix} \Gamma & \tau \\ \tau & \Gamma \end{bmatrix} \tag{6}$$

$$N = \begin{bmatrix} \kappa_{fd} & \kappa_{bd} \\ \kappa_{bd} & \kappa_{fd} \end{bmatrix} \tag{7}$$

$$P = \begin{bmatrix} \kappa_{fd} & \kappa_{bd} \\ \kappa_{bd} & \kappa_{fd} \end{bmatrix} \tag{8}$$

$$Q = \begin{bmatrix} \Gamma & \tau \\ \tau & \Gamma \end{bmatrix} \tag{9}$$

Since port 3 and port 4 are connected to make a loop as a ring resonator, the relationship between port 3 and port 4 can be described as:

$$\begin{bmatrix} a_{3N} \\ a_4 \end{bmatrix} = S_{cable} \begin{bmatrix} b_{3N} \\ b_4 \end{bmatrix} = \begin{bmatrix} 0 & e^{\gamma l} \\ e^{\gamma l} & 0 \end{bmatrix} \begin{bmatrix} b_{3N} \\ b_4 \end{bmatrix} \tag{10}$$

From (5) to (10), the relation between incident voltage and reflected voltage satisfy the following equation which is the actual coaxial cable ring resonator's S-parameter function:

$$S_{\text{resonator}} = \begin{bmatrix} S_{rr}^{11} & S_{rr}^{12} \\ S_{rr}^{21} & S_{rr}^{22} \end{bmatrix} = M + N\left[S_{cable}^{-1} - Q\right]^{-1} P \tag{11}$$

After expanding the equation, the reflection and transmission of the coaxial cable ring resonator can be written as (12) – (13):

$$S_{rr}^{11} = \Gamma + \frac{e^{2\gamma l}[2\kappa_{fd}\kappa_{bd}\lambda - \Gamma(\kappa_{fd}{}^2 + \kappa_{bd}{}^2)] - 2e^{\gamma l}\kappa_{fd}\kappa_{bd}}{e^{2\gamma l}\Gamma^2 - (1 - e^{\gamma l}\lambda)^2} \tag{12}$$

$$S_{rr}^{12} = \lambda + \frac{e^{2\gamma l}[-2\kappa_{fd}\kappa_{bd}\Gamma + \lambda(\kappa_{fd}{}^2 + \kappa_{bd}{}^2)] - e^{\gamma l}(\kappa_{fd}{}^2 + \kappa_{bd}{}^2)}{e^{2\gamma l}\Gamma^2 - (1 - e^{\gamma l}\lambda)^2} \tag{13}$$

To numerically calculate the transmission spectra of CCRR, we set the length of the cable to be 10 m and the frequency was interrogated from 10 kHz to 6 GHz. By substituting the S-matrix of CCBG calculated through Eq. (1)-(3), Figure 4 is the reflection spectrum of CCRR and the plot of transmission spectrum of CCRR as a function of frequency is shown in Figure 5 (a). It is interesting that the resonance peak strength increases at first and then slightly decreases as frequency increases. This phenomenon can be theoretically explained by critical coupling principle similar to

optical ring resonator. Figure 5 (b) plots the zoom-in spectrum of CCRR from 4 GHz to 5

GHz. The resonance can reach its largest strength at 4.52 GHz, and SNR is about 39 dB

indicating that the CCRR can be potentially a goof sensor device with high performance.

The effective loss propagation constant (α) of cable ring is related to the critical coupling.

The critical coupling means that most of the energy from input can be coupled to the

resonator system and SNR reaches its maximum when the internal loss is equal to the

coupling ratio. The CCRR system reaches critical coupling by setting α as a constant of

0.026, indicating its potential as a microwave band-stop filter. We can control coupling

coefficient by changing the number of holes along the CCBG-SC, then we have a basis
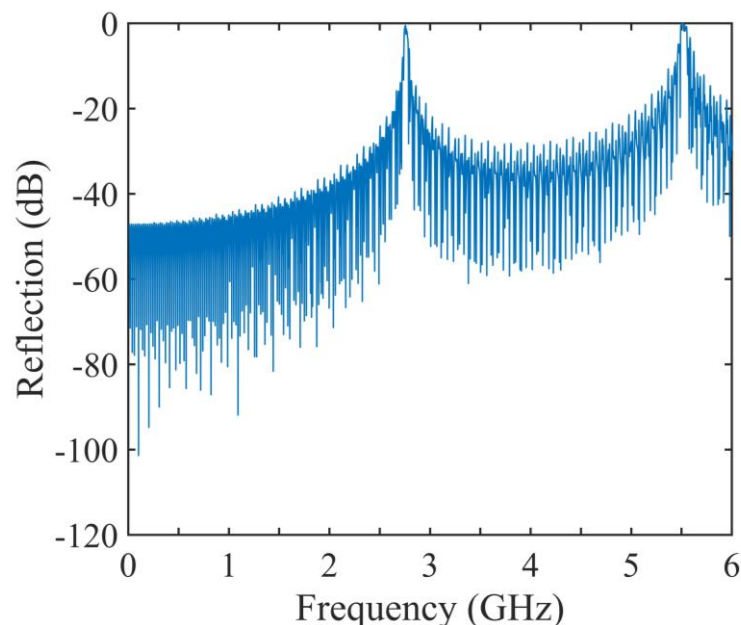
for a switching technology.
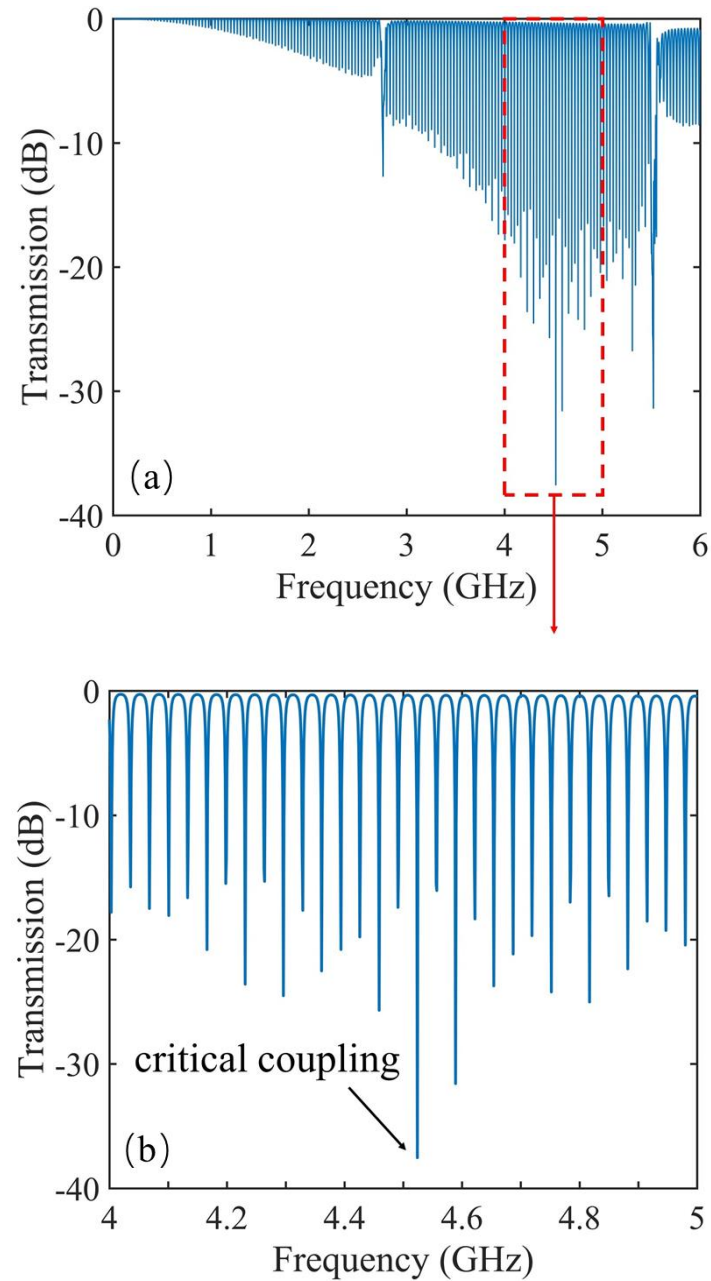

Figure 4. Calculated reflection spectrum of CCRR

Figure 5. Calculated spectrum of transmission of CCRR (a) Total spectrum of transmission from 10 kHz to 6 GHz (b) Zoomed transmission spectrum at critical coupling

3. EXPERIMENT RESULT

3.1. EXPERIMENT SETUP

In the demonstration experiment, two coaxial cables (RG-58/U, 50Ω) was fabricated by a computer numerical controlled (CNC) milling machine (Sherline P/N 8020A Model 2000). A milling bit of 3/16-inch diameter was used to periodically mill several circular holes vertically from first cable to the second cable. The inner conductors of coaxial cables were complete without any breaking. The period of hole-hole distance (Bragg period) was 38mm and the depth of the hole was 2.25mm which is nearly half of the cable diameter (4.95mm). A total number of 133 holes were fabricated in each cable. These two perpendicular cables perform like a coupler, coupling the EM wave from one cable to another cable. To obtain the RF response from the proposed CCRR, a vector network analyzer (VNA, HP8753ES) was used to monitor the transmission spectrum during experiment. The observation bandwidth was from 10 kHz to 6 GHz and the sampling points were spaced equally as 1601. The intermediate frequency bandwidth was 300 Hz.

3.2. TRANSMISSION SPECTRUM

The comparing of calculated transmission spectrum and experiment transmission spectrum is plotted in Figure 6. As the figure shown, the measurement results match well the spectrum in theory. Due to the loss associated with the background frequency, the overall trend of the transmitted spectrum decreases. As the length of coaxial cable ring

increases, the loss increases. The measurement transmission spectrum of CCRR based on CCGB-SC meets well with the algorithm.

Figure 7 (a) shows the transmission spectrum of the CCRR system. The fundamental resonance frequency and second-order harmonics of the CCBG can be observed. Multiple resonance frequency can be observed due to the wave travel in the ring resonator. The spectrum indicates the fundamental frequency is 2.76 GHz, which satisfies with the Bragg condition calculation. Figure 7 (b) plots the zooming part of critical coupling. Like typical fiber optic ring resonators, the coupling strength can be multiplied to reach critical coupling. At the frequency about around 4.6 GHZ, the resonance strength is large which over 52 dB, indicating energy in the ring is optimal.
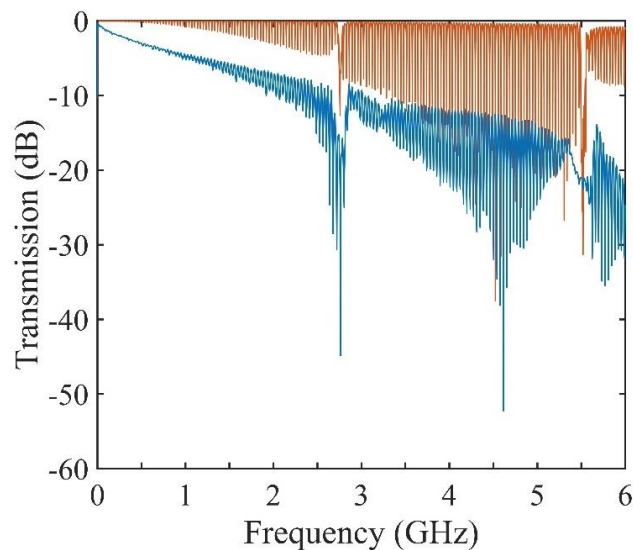

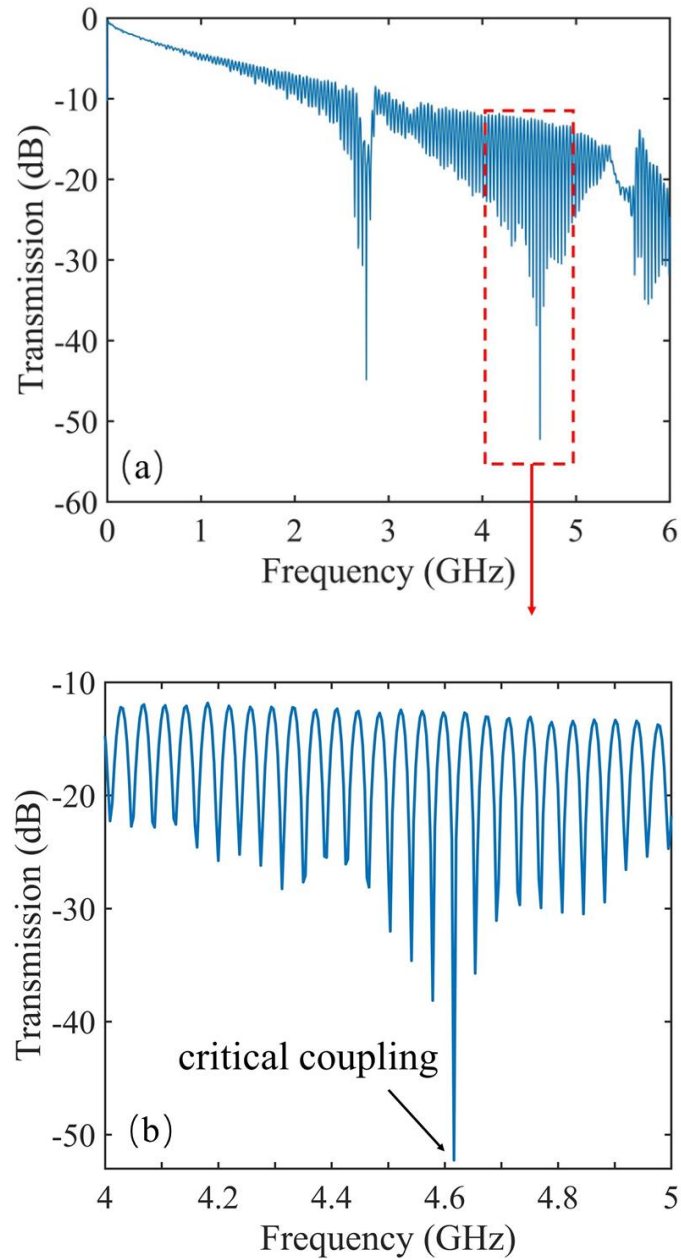Figure 6. Comparing of calculated transmission spectrum of CCRR and measured transmission spectrum of CCRR

Figure 7. Measured transmission spectrum of CCRR (a) Total transmission spectrum of CCRR with 133 holes from 10 kHz to 6 GHz (b) Zoomed measurement transmission spectrum at critical coupling

3.3. TEMPERATURE MEASUREMENT

To investigate CCRR for temperature sensing, we placed the coaxial cable into a tubular furnace and left other parts outside of the furnace. According to the datasheet of the coaxial cable, the environmental specifications Temperature Operating Range is from -40 °C to +100 °C, so in this experiment, the temperature was changed from 30°C to 100°C with a step of 10 °C. The rising time of each step was set to be 5 °C/min During each step, VNA was used to record spectra with an observation bandwidth from 4.64 GHz to 4.80 GHz. Figure 8 shows the change in transmission spectrum of CCRR for temperature sensing. As can be seen, the Q-factor doesn't decrease a lot indicating that the increasing temperature did not incur a noticeable loss to the cable.

According to the experiment results, when the temperature increases, the spectrum shifts to higher frequency region indicating the effective length of cable resonator decreases. Figure 9 plots the resonant frequency shift in response to the applied temperature, where the frequency shift increases non-linearly as the increase of applied temperature. The insert of Figure 9 plots the change of resonance frequency around 4.6 GHz as the ambient temperature increases. The temperature sensitivity of the system is about 60 kHz/°C. The results show the capability of CCRR for temperature sensing application.

There is one limitation of CCRR sensor is that after temperature sensing, the length of coaxial cable couldn't go back to its original length by leaving the cable at room temperature, which indicates the temperature leads to the change of length so the CCRR sensing part needs a better way to protect.
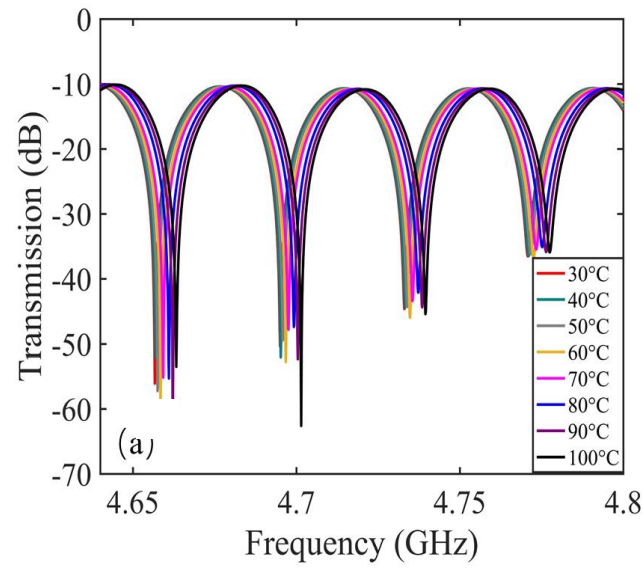
Figure 8. Change in transmission spectra in response to the ambient temperature
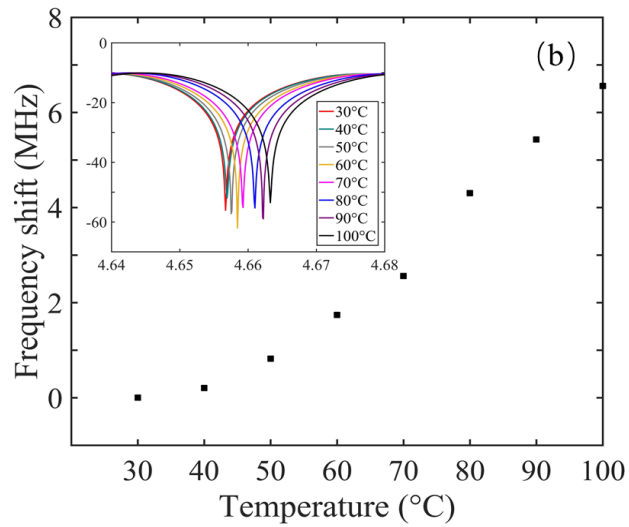

Figure 9. Frequency shift of the transmission spectra as a function of temperature
.

3.4. STRAIN MEASUREMENT

We also conducted strain measurement of the CCRR to further demonstrate capability of CCRR as a large strain sensing device in SHM. The CCRR was mounted on two translation stages. The reflection spectra of the CCBG shows no difference with or without stages, which indicates that stages did not introduce noticeable impedance mismatch and reflection. Similarly, the VNA was configured to acquire the transmission spectra with an observation bandwidth from 4.43 GHz to 4.64 GHz with a total sampling point of 1601. The load frame elongates the CCRR as a step of 3.95 mm, corresponding to a strain increase of about 3.95 mε as the initial sensing length is 1 m. Seven loading steps or a total strain of about 21.95 mε were applied to the CCRR. For each strain point, the transmission spectrum was measured multiple times consecutively to acquire the average spectrum.
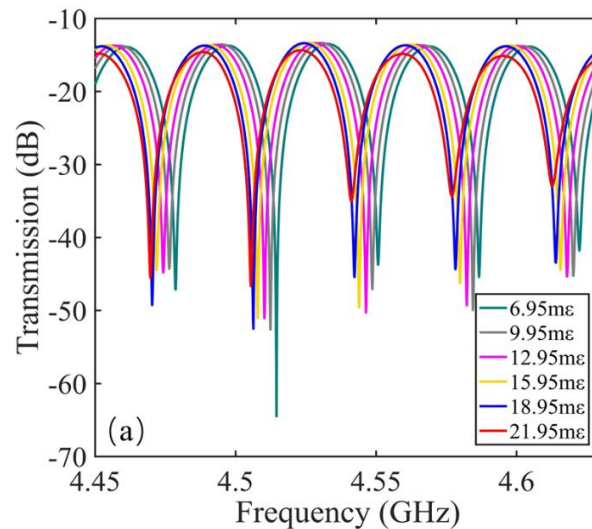

Figure 10. Amplitude of transmission spectra change with strain

Figure 10 plots the change of spectrum with respect to frequency with applied strain. The increasing strain to coaxial cable didn't incur a noticeable loss to the transmission spectra. The spectrum shifts to lower frequency region. Figure 11 plots the frequency shift as a function of the applied strain. The resonance frequency decreases almost linearly as a slope of -0.75 MHz/mε. The insert of Figure 11 is the change in resonance frequency at about 4.55 GHz. The SNR of resonance increased first and then decreased, which indicates the change of length introduce loss to the cable. When effective loss is equal to the transmission coefficient, the SNR reaches largest. The coaxial cable could survive over 21 mε (2.1%). It is easy to understand that once we apply strain to cable, the increase of length of the ring resonator results a decrease of resonance frequency. Even with strain as small as 0.5mε, CCRR sensor also performs well. The frequency shift is obvious to be recognized. The measurement was performed constant room temperature setting.
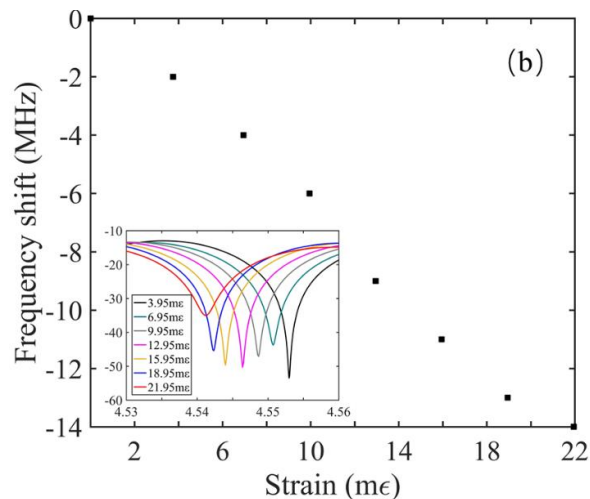

Figure 11. The resonance frequency shift as a function of strain

REFERENCES

[1] D. A. Krohn, T. MacDougall, and A. Mendez, Fiber optic sensors: fundamentals and applications. Spie Press Bellingham, WA, 2014.

[2] K. O. Hill and G. Meltz, "Fiber Bragg grating technology fundamentals and overview," Journal of lightwave technology, vol. 15, no. 8, pp. 1263-1276, 1997.

[3] S. W. James and R. P. Tatam, "Optical fibre long-period grating sensors: characteristics and application," Measurement science and technology, vol. 14, no. 5, p. R49, 2003.

[4] P. Morris, A. Hurrell, A. Shaw, E. Zhang, and P. Beard, "A Fabry–Pérot fiber-optic ultrasonic hydrophone for the simultaneous measurement of temperature and acoustic pressure," The Journal of the Acoustical Society of America, vol. 125, no. 6, pp. 3611-3622, 2009.

[5] J. H. Lim, H. S. Jang, K. S. Lee, J. C. Kim, and B. H. Lee, "Mach–Zehnder interferometer formed in a photonic crystal fiber based on a pair of long-period fiber gratings," Optics Letters, vol. 29, no. 4, pp. 346-348, 2004.

[6] L.-b. Yuan, L.-m. Zhou, and J.-s. Wu, "Fiber optic temperature sensor with duplex Michleson interferometric technique," Sensors and Actuators A: Physical, vol. 86, no. 1-2, pp. 2-7, 2000.

[7] A. Yariv, "Critical coupling and its control in optical waveguide-ring resonator systems," IEEE Photonics Technology Letters, vol. 14, no. 4, pp. 483-485, 2002.

[8] S. Doiron, C. Giller, N. Beaudoin, and A. Haché, "A periodic structure for electronic signals and demonstration of electronic lasing," American Journal of Physics, vol. 76, no. 11, pp. 996-1001, 2008.

[9] P. Bernard and J. Gautray, "Measurement of dielectric constant using a microstrip ring resonator," IEEE Transactions on Microwave Theory and Techniques, vol. 39, no. 3, pp. 592-595, 1991.

[10] I. Wolff, "Microstrip bandpass filter using degenerate modes of a microstrip ring resonator," Electronics Letters, vol. 8, no. 12, pp. 302-303, 1972.

[11] H. Zhu, I. M. White, J. D. Suter, M. Zourob, and X. Fan, "Opto-fluidic micro-ring resonator for sensitive label-free viral detection," Analyst, vol. 133, no. 3, pp. 356-360, 2008.

[12]   D. R. Smith, W. J. Padilla, D. Vier, S. C. Nemat-Nasser, and S. Schultz, "Composite medium with simultaneously negative permeability and permittivity," Physical review letters, vol. 84, no. 18, p. 4184, 2000.

[13]   H. Moser, B. Casse, O. Wilhelmi, and B. Saw, "Terahertz response of a microfabricated rod–split-ring-resonator electromagnetic metamaterial," Physical review letters, vol. 94, no. 6, p. 063901, 2005.

[14]   M. Silva-López et al., "Strain and temperature sensitivity of a single-mode polymer optical fiber," Optics letters, vol. 30, no. 23, pp. 3129-3131, 2005. [15] Wei, T., S. Wu, J. Huang, H. Xiao and J. Fan (2011). "Coaxial cable Bragg grating." Applied Physics Letters 99(11): 113517.

[15]   T. Wei, S. Wu, J. Huang, H. Xiao, and J. Fan, "Coaxial cable Bragg grating," Applied Physics Letters, vol. 99, no. 11, p. 113517, 2011.

[16]   J. Huang, T. Wang, L. Hua, J. Fan, H. Xiao, and M. Luo, "A coaxial cable Fabry-Perot interferometer for sensing applications," Sensors, vol. 13, no. 11, pp. 15252-15260, 2013.

[17]   C. Zhu, Y. Zhuang, Y. Chen, and J. Huang, "A hollow coaxial cable Fabry–Pérot resonator for liquid dielectric constant measurement," Review of Scientific Instruments, vol. 89, no. 4, p. 045003, 2018.

[18]   J. Huang, T. Wei, T. Wang, J. Fan, and H. Xiao, "Control of critical coupling in a coiled coaxial cable resonator," Review of scientific instruments, vol. 85, no. 5, p. 054701, 2014.

[19]   J. Huang, T. Wei, X. Lan, J. Fan, and H. Xiao, "Coaxial cable Bragg grating sensors for large strain measurement with high accuracy," in Sensors and Smart Structures Technologies for Civil, Mechanical, and Aerospace Systems 2012, 2012, vol. 8345, p. 83452Z: International Society for Optics and Photonics.

[20]   J. Pan, X. Gao, C. Sui, J. Fan, Z. Yang, and K. Wu, "S-parameter estimation algorithm for coaxial ring resonator," in Electromagnetic Compatibility (EMC), 2016 IEEE International Symposium on, 2016, pp. 775-779: IEEE.

[22]   J. A. Davis, D. A. Miller, M. d. M. Sánchez-López, and J. Cos, "Multiple-beam interference with coaxial cable analogs of optical arrays," American journal of physics, vol. 74, no. 12, pp. 1066-1070, 2006.

[21]   J. Huang, T. Wei, J. Fan, and H. Xiao, "Coaxial cable Bragg grating assisted microwave coupler," Review of scientific instruments, vol. 85, no. 1, p. 014703, 2014.

[23]   S. Wu, T. Wei, J. Huang, H. Xiao, and J. Fan, "A study on Q-factor of CCBG sensors by coupled mode theory," in Sensors and Smart Structures Technologies for Civil, Mechanical, and Aerospace Systems 2012, 2012, vol. 8345, p. 834549: International Society for Optics and Photonics.

SECTION

3. CONCLUSION

To summarize, a CCRR was proposed, which was demonstrated by producing a homemade CCBG-SC and then connecting two ports to make a ring resonator. Comparing to the commercial coupler, CCBG-SC improves the flexibility of the device for sensing applications. By control the number and of the grating and the distance between holes, the critical coupling can be observed. A theoretical model was developed to better understand the physics of CCRR. The S-parameter of CCBG was calculated using finite element method. The transmission spectrum of CCRR was calculated using an estimated algorithm. All the theoretical calculations agree with the measurement results. A resonance strength of 39 dB at 4.62 GHz was observed in the device indicating the capability of sensing application. The experimental results match well with the theoretically calculated results. Temperature measurement was experimentally demonstrated, and the sensitivity is about 60 kHz/°C. We also conducted a strain measurement of CCRR. The resonant frequency of the CCRR device indicated approximately linear responses of -750 kHz/mε to the loaded strain and coaxial cable can survive up to 21 mε. Comparing to the FRR system, CCRR sensing system offers improvements of performance and largely reduces costs by minimizing the requirements for insulation. The CCRR concept could lead to measure various parameters such a monitoring of displacement, pressure, material property, liquid level, etc.

BIBLIOGRAPHY

[1]   Q. Ling, Z. Tian, Y. Yin, and Y. Li, "Localized structural health monitoring using energy-efficient wireless sensor networks," IEEE Sensors Journal, vol. 9, no. 11, pp. 1596-1604, 2009.

[2]   A. Gómez González, E. Zugasti, and J. Anduaga, "Damage Identification in a Laboratory Offshore Wind Turbine Demonstrator," in Key Engineering Materials, 2013, vol. 569, pp. 555-562: Trans Tech Publ.

[3]   http://www.iste.co.uk/data/doc_xqjujdlhnfls.pdf.

[4]   T. Zhu, D. Wu, M. Liu, and D.-W. Duan, "In-line fiber optic interferometric sensors in single-mode fibers," Sensors, vol. 12, no. 8, pp. 10430-10449, 2012.

[5]   T. Vandiver, "Health monitoring of US army missile systems," Structural Health Monitoring, Current Status and Perspectives, pp. 191-196, 1997.

[6]   K. Chintalapudi et al., "Monitoring civil structures with a wireless sensor network," IEEE Internet Computing, vol. 10, no. 2, pp. 26-34, 2006.

[7]   A. Othonos, "Fiber bragg gratings," Review of scientific instruments, vol. 68, no. 12, pp. 4309-4341, 1997.

[8]   M. Wegmuller, J. Von Der Weid, P. Oberson, and N. Gisin, "High resolution fiber distributed measurements with coherent OFDR," in Proc. ECOC'00, 2000, vol. 11, no. 4, p. 109: Munich, Germany.

[9]   S. Rizzolo et al., "Evaluation of Distributed OFDR-Based Sensing Performance in Mixed Neutron/Gamma Radiation Environments," IEEE Transactions on Nuclear Science, vol. 64, no. 1, pp. 61-67, 2017.

[10]   L. Alwis, T. Sun, and K. Grattan, "Optical fibre-based sensor technology for humidity and moisture measurement: Review of recent progress," Measurement, vol. 46, no. 10, pp. 4052-4074, 2013.

[11]   S. Yin and T. Francis, Fiber optic sensors. CRC press, 2002.

[12]   H.-N. Li, D.-S. Li, and G.-B. Song, "Recent applications of fiber optic sensors to health monitoring in civil engineering," Engineering structures, vol. 26, no. 11, pp. 1647-1657, 2004.

[13]   F. Zhang and J. W. Lit, "Direct-coupling single-mode fiber ring resonator," JOSA A, vol. 5, no. 8, pp. 1347-1355, 1988.

[14]   L. F. Stokes, M. Chodorow, and H. J. Shaw, "All-single-mode fiber resonator," Optics Letters, vol. 7, no. 6, pp. 288-290, 1982.

[15]   J. E. Heebner, V. Wong, A. Schweinsberg, R. W. Boyd, and D. J. Jackson, "Optical transmission characteristics of fiber ring resonators," IEEE journal of quantum electronics, vol. 40, no. 6, pp. 726-730, 2004.

[16]   J. Zubia and J. Arrue, "Plastic optical fibers: An introduction to their technological processes and applications," Optical fiber technology, vol. 7, no. 2, pp. 101-140, 2001.

[17]   J. Huang, T. Wang, L. Hua, J. Fan, H. Xiao, and M. Luo, "A coaxial cable Fabry-Perot interferometer for sensing applications," Sensors, vol. 13, no. 11, pp. 15252-15260, 2013.

[18]   S. Sun et al., "A novel TDR-based coaxial cable sensor for crack/strain sensing in reinforced concrete structures," 2009.

[19]   J. Pan, X. Gao, C. Sui, J. Fan, Z. Yang, and K. Wu, "S-parameter estimation algorithm for coaxial ring resonator," in Electromagnetic Compatibility (EMC), 2016 IEEE International Symposium on, 2016, pp. 775-779: IEEE.

[20]   T. Wei, S. Wu, J. Huang, H. Xiao, and J. Fan, "Coaxial cable Bragg grating," Applied Physics Letters, vol. 99, no. 11, p. 113517, 2011.

[21]   J. Huang, T. Wei, J. Fan, and H. Xiao, "Coaxial cable Bragg grating assisted microwave coupler," Review of scientific instruments, vol. 85, no. 1, p. 014703, 2014.

VITA

Xiaotong Tang obtained her bachelor's degree in the school of Electrical Information Engineering of Northeastern University at Qinhuangdao in June 2016. In August 2016, she joined the graduate program in the Department of Electrical and Computer Engineering at Missouri University of Science and Technology. Her research interest focused on coaxial cable sensors. She received a Master of Science in Electrical Engineering from Missouri University of Science and Technology in December 2018.